



Measurement of CP violation in $B^0 \rightarrow \psi(\rightarrow \ell^+ \ell^-) K_S^0(\rightarrow \pi^+ \pi^-)$ decays

LHCb collaboration[†]

Abstract

A measurement of time-dependent CP violation in the decays of B^0 and \bar{B}^0 mesons to the final states $J/\psi(\rightarrow \mu^+ \mu^-) K_S^0$, $\psi(2S)(\rightarrow \mu^+ \mu^-) K_S^0$ and $J/\psi(\rightarrow e^+ e^-) K_S^0$ with $K_S^0 \rightarrow \pi^+ \pi^-$ is presented. The data correspond to an integrated luminosity of 6 fb^{-1} collected at a center-of-mass energy of $\sqrt{s} = 13 \text{ TeV}$ with the LHCb detector. The CP -violation parameters are measured to be

$$S_{\psi K_S^0} = 0.717 \pm 0.013 (\text{stat}) \pm 0.008 (\text{syst}),$$

$$C_{\psi K_S^0} = 0.008 \pm 0.012 (\text{stat}) \pm 0.003 (\text{syst}).$$

This measurement of $S_{\psi K_S^0}$ represents the most precise single measurement of the CKM angle β to date and is more precise than the current world average. In addition, measurements of the CP -violation parameters of the individual channels are reported and a combination with the LHCb Run 1 measurements is performed.

Published in Phys. Rev. Lett. 132 (2024) 021801

© 2024 CERN for the benefit of the LHCb collaboration. CC BY 4.0 licence.

[†]Authors are listed at the end of this Letter.

Charge-parity (CP) symmetry violation in transitions of neutral mesons to CP -invariant final states can occur in the interference of the decay amplitudes with and without neutral meson mixing. The $B^0 \rightarrow \psi K_S^0$ decays involving charmonium states, $\psi = [J/\psi, \psi(2S)]$, are dominated by the $b \rightarrow c\bar{c}s$ tree-level transition and have a clean experimental signature. Measurements of CP violation in neutral meson decays to charmonium final states have thus resulted in a high degree of precision for the angle β of the Cabibbo Kobayashi Maskawa (CKM) matrix: $\sin(2\beta) = 0.699 \pm 0.017$ [1]. The first observation of CP violation in the B -meson system was reported in the $B^0 \rightarrow J/\psi K_S^0$ channel by the *BABAR* [2] and Belle [3] collaborations. The measurement of the CP -violation parameter $\sin(2\beta)$ has been updated several times by these experiments [4, 5] and more recently by the LHCb [6, 7] and Belle II [8] collaborations.

A measurement of CP violation in the interference of B^0 decays with and without mixing entails the measurement of the periodic change of decay-rate differences of initial B^0 and \bar{B}^0 mesons to a common, CP -invariant final state, f , with time. The underlying decay-time-dependent CP asymmetry can be expressed as

$$\mathcal{A}^{CP}(t) = \frac{\Gamma(\bar{B}^0(t) \rightarrow f) - \Gamma(B^0(t) \rightarrow f)}{\Gamma(\bar{B}^0(t) \rightarrow f) + \Gamma(B^0(t) \rightarrow f)} = \frac{S \sin(\Delta m_d t) - C \cos(\Delta m_d t)}{\cosh(\frac{1}{2}\Delta\Gamma_d t) + \mathcal{A}_{\Delta\Gamma} \sinh(\frac{1}{2}\Delta\Gamma_d t)}, \quad (1)$$

where S , C , and $\mathcal{A}_{\Delta\Gamma}$ are the CP -violation parameters and Δm_d is the B^0 - \bar{B}^0 mixing frequency [9]. The parameter S can be related to the CKM angle β as $S = \sin(2\beta + \Delta\phi_d + \Delta\phi_d^{\text{NP}})$, where $\Delta\phi_d^{\text{NP}}$ is a possible contribution from physics beyond the standard model. Contributions from penguin topologies to the decay amplitude that cause an additional phase shift $\Delta\phi_d$ are CKM suppressed, hence deviations of S from $\sin(2\beta)$ are expected to be small in the standard model [11–16]. In this measurement it is assumed that the width difference between B mass eigenstates, $\Delta\Gamma_d$, is compatible with zero [1], such that the denominator on the right-hand side of Eq. (1) is equal to one.

The LHCb detector [17, 18] is a single-arm spectrometer covering the forward pseudo-rapidity region, designed for the study of particles containing b or c quarks. The detector elements that are particularly relevant to this measurement are a silicon-strip vertex locator (VELO) surrounding the proton-proton (pp) interaction region that allows c and b hadrons to be identified from their characteristically long flight distance; a tracking system that consists of a dipole magnet and sets of tracking stations before and after the magnet, and provides a measurement of the momentum, p , of charged particles; and two ring-imaging Cherenkov detectors (RICH) that are able to discriminate between different species of charged hadrons. In addition, a muon system allows the identification of muons, and a calorimeter system provides electron identification. The online event selection is performed by a trigger [19], which consists of a hardware stage, based on information from the calorimeter and muon systems, followed by a software stage, which applies a full event reconstruction.

The measurements reported in this Letter use the pp collision data collected by the LHCb experiment during Run 2 (2015 to 2018) at a center-of-mass energy of 13 TeV. The three decay modes $B^0 \rightarrow J/\psi(\rightarrow \mu^+\mu^-)K_S^0$, $B^0 \rightarrow \psi(2S)(\rightarrow \mu^+\mu^-)K_S^0$, and $B^0 \rightarrow J/\psi(\rightarrow e^+e^-)K_S^0$, with $K_S^0 \rightarrow \pi^+\pi^-$, are studied, and a combined, time-dependent maximum-likelihood fit is performed to measure the CP -violation parameters. To select the signal modes, trigger decisions associated with particles reconstructed off-line are applied, and requirements are made on whether the decision was caused by the reconstructed signal candidate, by other reconstructed particles in the event, or both. For the

dimuon channels, only candidates responsible for the muon trigger decision are considered. For the reconstruction of $\psi \rightarrow \mu^+ \mu^-$ candidates, muons with momentum transverse to the beam direction, p_T , larger than 500 MeV/c are required to form a good-quality vertex. The dimuon invariant mass must be within ± 100 MeV/c² of the known J/ψ or $\psi(2S)$ masses [10]. For the selection of $J/\psi \rightarrow e^+ e^-$ candidates, all events selected by the trigger are considered. The two electron candidates are required to have $p_T > 500$ MeV/c and to form a good-quality vertex. The dielectron invariant mass is required to be in the range [2300, 3300] MeV/c². The final-state K_S^0 meson is reconstructed from two tracks forming a good-quality vertex.

Because of its long flight distance, about two thirds of all $K_S^0 \rightarrow \pi^+ \pi^-$ decays occur downstream of the VELO but before the next tracking subdetector, the tracker turicensis (TT), which is located upstream of the LHCb magnet. Tracks that are reconstructed from hits in the VELO as well as by subsequent LHCb tracking detectors are called long (L). Tracks that are only measured by the TT and the tracking stations are called downstream (D). Consequently a K_S^0 candidate can be reconstructed as a “ LL ”, “ DD ”, or “ LD ” track combination. In addition, upstream (U) tracks, which are only measured by the VELO and TT and then bent out of the LHCb acceptance due to their low momentum, are included and matched to a L track to form a “ UL ” K_S^0 candidate. L and D tracks are required to have momenta above 2 GeV/c whereas for U tracks the requirement is lower, at 1 GeV/c. Moreover, the two tracks are required to have a reconstructed invariant mass within ± 80 MeV/c² of the known K_S^0 mass [10]. The K_S^0 reconstruction categories LD and UL are included for the first time in a measurement of time-dependent CP violation at LHCb and add 13% to the signal yield of the $B^0 \rightarrow J/\psi(\rightarrow \mu^+ \mu^-) K_S^0$ mode. As the precision of the measured dimuon vertex determines the decay-time precision and does not depend on the kaon reconstruction, the new reconstruction categories were found to be as well suited for the measurement as the LL and DD categories. The signal B^0 candidates are formed from reconstructed K_S^0 and ψ candidates forming a good-quality vertex, which is displaced from the primary pp interaction vertex (PV). Because of the inclusive trigger approach used for the dielectron channel, an additional off-line selection is applied to reduce the background level. Reduced K_S^0 mass windows of 25 MeV/c² and 33 MeV/c² are chosen for LL and DD K_S^0 candidates, and a more stringent requirement on the alignment between the B momentum vector and the direction defined by the PV and B decay vertex is applied.

Background due to $\Lambda_b^0 \rightarrow \psi \Lambda(\rightarrow p \pi^-)$ decays where the proton is misidentified as a pion is suppressed by removing candidates with the recalculated proton-pion invariant mass in the range [1110, 1130] MeV/c² and a poor pion identification likelihood, as measured by the RICH detectors. Background contributions from decays involving short-lived intermediate hadronic resonances like $B^0 \rightarrow \psi K^{*0}$ with a misidentified charged kaon are suppressed by requiring that the reconstructed K_S^0 decay time exceeds 0.5 ps. In the following, K^{*0} denotes the resonance $K^*(892)^0$. The $B^+ \rightarrow \psi K^+$ decay can also mimic the signal if an extra low-momentum U -track pion is combined with the misidentified charged kaon. This source of background contribution is reduced by requiring that the pion candidates have low kaon-identification likelihoods.

The background due to random track combinations, named combinatorial background, is reduced with a boosted decision tree classifier (BDT) [20]. This model is trained on simulated $B^0 \rightarrow \psi K_S^0$ decays as the signal proxy and B -meson candidates with $m(\psi K_S^0) > 5400$ MeV/c² as the background proxy. In the simulation, the pp collisions are

generated with the event-generator PYTHIA [21] with a specific LHCb configuration [22]. The material interaction in the detector is simulated with the GEANT4 toolkit [23]. Decays of unstable particles are simulated with EVTGEN [24] with a phase-space model including CP violation, in which final-state radiation is generated using PHOTOS [25]. The training features show good agreement between background-subtracted data and simulation. They include the impact parameter of the reconstructed B^0 , ψ , and K_S^0 candidates, defined as the shortest distance between each particle’s reconstructed trajectory and the PV, the p_T of the K_S^0 and π^\pm mesons and the K_S^0 pseudorapidity. A kinematic fit to the signal decay tree where the ψ and K_S^0 masses are constrained to their known values is performed, and the resulting fit χ^2 is added to the set of training features. To minimize overtraining, a k -folding technique [26] is used with $k = 5$ and the training is stopped as soon as the classifiers’ separation power no longer significantly improves on the test sample. The predictions of the BDTs trained on the five folds are averaged. The BDT classifiers are trained separately for each K_S^0 reconstruction class. The selection is finalized by applying a requirement on the BDT output that maximizes the signal yield sensitivity. Following the selection procedure, 0.7% of events contain multiple signal candidates; in these cases the candidate with the highest p_T is selected.

The flavor of the B meson at production, needed to evaluate Eq. (1), is determined by different methods that either exploit additional particles produced in the fragmentation of the b quark associated with the signal- B meson (same side tagging, SS) or from the decay of the b hadron produced in association with the signal (opposite side tagging, OS). The particles considered in these processes include protons and pions from the signal b -quark fragmentation process, and kaons, electrons, muons and reconstructed charged charm-hadron decays as well as a weighted mean of the charges of all reconstructed decay vertices of the associated partner b -hadron decay. Collectively, these methods are referred to as flavor tagging (FT) [27, 28]. From the measured particle charges, the initial B state can be inferred in the form of a tagging decision $d = (+1, -1) \equiv (B^0, \bar{B}^0)$. In addition, a probability estimate that the assigned decision is wrong (predicted mistag or η) is estimated for each candidate by means of a multivariate classification method.

The predicted mistag is calibrated by means of a dedicated software package [29], using flavor-specific channels that are kinematically similar to the signal channels, to guarantee the calibrated mistag function, $\omega(\eta)$, closely matches the mistag probability in the calibration channels. The difference in the tagging response for \bar{B}^0 and B^0 mesons is taken into account with separate calibrated tagging responses $\omega^-(\eta)$ and $\omega^+(\eta)$, respectively. Two calibration channels are considered in this analysis: the $B^+ \rightarrow J/\psi K^+$ and $B^0 \rightarrow J/\psi K^{*0} (\rightarrow K^+ \pi^-)$ decays where the J/ψ is either reconstructed from two electrons or two muons, depending on the targeted signal mode. Selection criteria similar to the signal requirements are applied and weights to subtract background contributions are determined from a fit to the B candidates invariant mass distribution with the sPlot method [30, 31]. Before calibrating the tagging output, the samples are weighted such that the relevant candidate kinematic distributions and properties match those of the corresponding B candidates in the signal decay modes. These distributions and properties are the B candidate pseudorapidity, p_T and azimuth angle, and the number of reconstructed PVs and tracks in each event. After the calibration of individual tagging algorithms, the OS and SS combinations are calibrated using both control channels.

The final FT calibration parameters are determined from a fit to the decay-time distribution of the $B^0 \rightarrow J/\psi K^{*0}$ signal candidates where constraints on the OS parameters

Table 1: Flavor tagging efficiency and \mathcal{D}^2 factor for each decay channel.

Channel	$\epsilon_{\text{tag}} [\%]$	$\mathcal{D}^2 [\%]$
$B^0 \rightarrow J/\psi(\rightarrow \mu^+\mu^-)K_S^0$	85.34 ± 0.05	4.661 ± 0.013
$B^0 \rightarrow J/\psi(\rightarrow e^+e^-)K_S^0$	92.20 ± 0.08	6.462 ± 0.032
$B^0 \rightarrow \psi(2S)(\rightarrow \mu^+\mu^-)K_S^0$	84.81 ± 0.15	4.59 ± 0.04

from the $B^+ \rightarrow J/\psi K^+$ calibration are applied. In this fit the asymmetries of the B^0 - \bar{B}^0 production, $\alpha \equiv [N(\bar{B}^0) - N(B^0)]/[N(\bar{B}^0) + N(B^0)]$ and reconstruction, as well as of tagging efficiencies, defined here as $\Delta\epsilon_{\text{tag}} \equiv (\epsilon_{\text{tag}}^{\bar{B}^0} - \epsilon_{\text{tag}}^{B^0})/(\epsilon_{\text{tag}}^{\bar{B}^0} + \epsilon_{\text{tag}}^{B^0})$, are determined and production and tagging asymmetries are propagated to the signal fit. The tagging power measures the effective loss in signal yield compared to a perfectly tagged sample for a measurement of the time-dependent CP asymmetry. It is calculated as $\epsilon_{\text{tag}}\mathcal{D}^2$, where the tagging efficiency ϵ_{tag} is the fraction of tagged events in relation to the total sample size and \mathcal{D} is the FT dilution factor $[1 - 2\omega(\eta)]$. A summary of the values of ϵ_{tag} and \mathcal{D}^2 found for each considered decay is given in Table 1, and in the following, only events with available tagging decisions are considered. The tagging power depends on the selection criteria used to isolate each signal. For the dielectron mode, the stricter requirements imposed by the trigger and subsequent selection cause the tagging power to be higher than for the dimuon modes.

Unbinned, extended maximum-likelihood fits to the invariant-mass distributions of the signal candidates are performed for each final state to determine the signal and background contributions. From the result of these fits, sets of weights are determined using the sPlot method and are used to obtain the signal decay-time distributions from the data. The B^0 signal is described by a two-sided Hypatia probability density function (PDF) [32] in each channel. The Hypatia parameters defining the tails are determined from the respective simulation sample. The width and mean are allowed to float in the fit to the data. The same model and all its shape parameters are used to describe background B_s^0 decays into the same final states, but the mean, relative to that of the B^0 component, is offset by the known mass difference [10]. The combinatorial background is described by an exponential distribution and the partially reconstructed low-mass background is described by a Gaussian distribution.

Figure 1 shows the invariant mass distribution of the selected candidates of all the decay modes, with the full fit functions and their partial contributions. In total, $306\,090 \pm 570$, $23\,560 \pm 160$, and $42\,700 \pm 220$ signal decays with an identified flavor at production are found in the modes $B^0 \rightarrow J/\psi(\rightarrow \mu^+\mu^-)K_S^0$, $B^0 \rightarrow \psi(2S)(\rightarrow \mu^+\mu^-)K_S^0$ and $B^0 \rightarrow J/\psi(\rightarrow e^+e^-)K_S^0$, respectively.

The CP -violation parameters S and C are determined from a weighted maximum-likelihood fit to the time-dependent decay rates of B^0 and \bar{B}^0 tagged decays in the individual decay channels, after the results of individual years and reconstruction categories were found to be consistent. In addition, a simultaneous fit of all channels is performed using the same model. The time-dependent decay rate is expressed as

$$\mathcal{P}(t, d, \eta) \propto e^{-\Gamma t/h} \left\{ [1 + d(1 - 2\omega^+(\eta))] P_{B^0}(t) + [1 + d(1 - 2\omega^-(\eta))] P_{\bar{B}^0}(t) \right\} \quad (2)$$

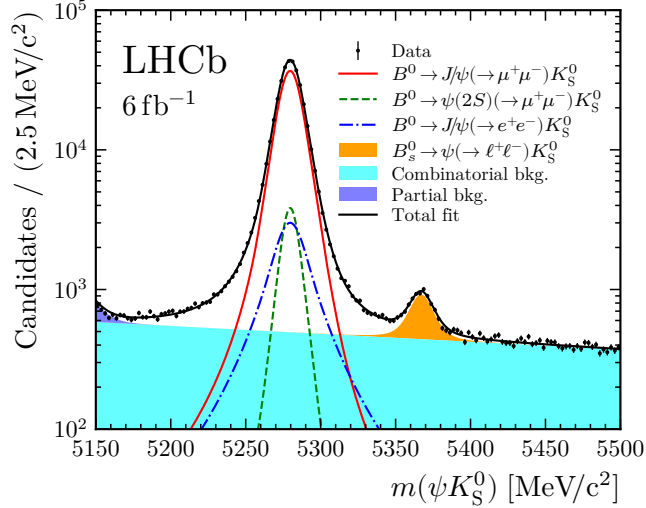


Figure 1: Invariant-mass distribution of the selected candidates with an identified flavor at production of the three signal channels.

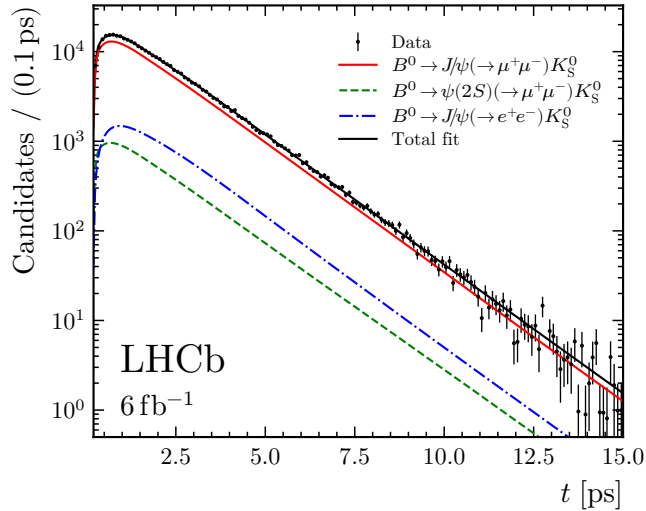


Figure 2: Decay-time distribution of the signal with an identified flavor at production, where the background is statistically subtracted by means of the sPlot method. The projections of the time-dependent fit for the individual contributions of the three decay modes and for the total are superimposed.

with

$$P_{B^0,(\bar{B}^0)}(t) \propto (1 \mp \alpha)(1 \mp \Delta\epsilon_{\text{tag}})[1 \mp S \sin(\Delta m_d t) \pm C \cos(\Delta m_d t)], \quad (3)$$

and where Γ_d is the B^0 decay width. The decay-time resolution is accounted for in the fit by convolving Eq. (2) with a decay-time resolution model that is validated on simulation, corresponding to an effective resolution of about 60 fs. The effect of the resolution on the CP -asymmetry amplitude is at the level of 0.5‰ and thus small compared to the statistical sensitivity. The resolution model consists of the sum of three Gaussian distributions centered at zero with widths defined as linear functions of the decay-time uncertainty. A possible bias in the decay-time reconstruction due to VELO misalignment

is considered and modeled by a second-degree polynomial of the decay-time uncertainty. The parameters of the model are determined from a fit to the decay-time distribution of a data sample made of $J/\psi\pi^+\pi^-$ candidates compatible with originating from the PV. The effect of the decay-time dependent signal-reconstruction efficiency is accounted for by multiplying the total PDF by a cubic spline model, whose shape is allowed to float in the fit. The parameters Δm_d and Γ_d are allowed to vary in the fit with Gaussian constraints to their known values [10]. Similarly, the FT calibration parameters and the production asymmetry are constrained to the $B^0 \rightarrow J/\psi K^{*0}$ fit results using the full covariance matrix. The effect of kaon regeneration and CP violation in the neutral kaon system on the CP -violation parameters of the B^0 system are estimated [33, 34] and applied as a correction for each mode. The correction assigned to the combined fit is $+0.0016$ for S and -0.0035 for C . Figure 2 shows the decay-time distribution of the signal candidates with the fit result overlaid. Figure 3 shows the corresponding CP asymmetry as a function of decay time, where the data points correspond to the maximum-likelihood estimator of the time-integrated CP asymmetry in each decay-time bin, defined as $\mathcal{A}_{\text{int}}^{CP} = -(\sum_j^N \kappa_j d_j D_j) / (\sum_j^N \kappa_j D_j^2)$, whereby $D_j = (1 - \omega_j^+ - \omega_j^-)$ is the tagging dilution, d_j is the tagging decision, and κ_j is the signal event weight obtained with the sPlot method.

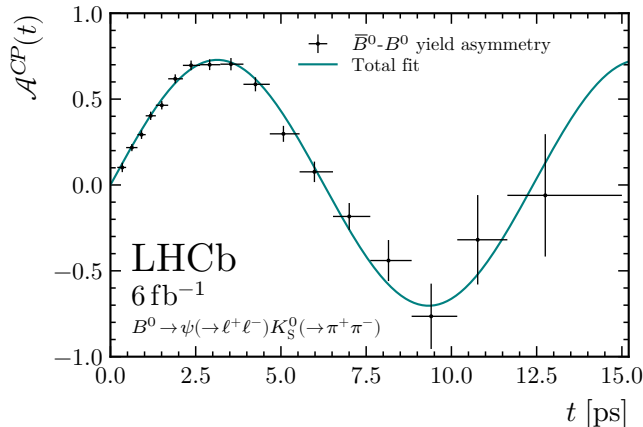


Figure 3: Time-dependent CP asymmetry from the maximum-likelihood estimator of the binned asymmetry with the fit result overlaid.

Several sources of systematic uncertainties on the CP -violating observables are investigated, including those associated with the choice of fit model and the uncertainty of the external inputs. The corresponding effects are studied using pseudoexperiments in which ensembles of pseudodata are generated using parameters that differ from those used in the baseline fit. The generated datasets are then fitted with the nominal model to test whether biases in the parameters of interest occur. Each contribution is evaluated separately in each signal mode. Sources of leading systematic uncertainty are listed in Table 2. A small bias in the result of the baseline fit is observed and assumed to be fully correlated among different signal modes. The resulting systematic uncertainty on the combined result is obtained from the arithmetic mean of individual decay channels. Other sources of systematic uncertainty are assumed to be uncorrelated. The total systematic uncertainty for the combined fit is a weighted average of the individual uncertainties, taking into account the sensitivity of each mode to the CP -violating parameters. The systematic uncertainty due

Table 2: Summary of systematic uncertainties on S and C . Each contribution is a weighted average of the uncertainties of the individual fits, except for the fitter validation.

Source	$\sigma(S)$	$\sigma(C)$
Fitter validation	0.0004	0.0006
Decay-time bias model	0.0007	0.0013
FT $\Delta\epsilon_{\text{tag}}$ portability	0.0014	0.0017
FT calibration portability	0.0053	0.0001
$\Delta\Gamma_d$ uncertainty	0.0055	0.0017

to the uncertainty of $\Delta\Gamma_d$ is obtained by analyzing pseudoexperiments generated with input values shifted by $+1\sigma$ and -1σ from its assumed central value of zero, where σ is the sum of the current world average uncertainty and absolute central value. The larger deviation is chosen as the systematic uncertainty. Small differences in the FT calibration parameters and in the tagging efficiency asymmetry between the control channels and the signal modes are observed in simulation (FT calibration portability). The contribution due to the portability of the FT calibration is evaluated by analyzing pseudoexperiments accounting for the different calibration values at generation level. The systematic uncertainty due to the observed $\Delta\epsilon_{\text{tag}}$ differences in simulation is evaluated from the fit to data with modified input values. Uncertainties on the parameters of the decay-time bias correction function are evaluated with pseudoexperiments, where the parameters are varied within their uncertainties. The uncertainty of Δm_d is included in the statistical uncertainty and its isolated contribution to the combined fit is $\sigma_{\Delta m_d}(S) = 0.0004$ and $\sigma_{\Delta m_d}(C) = 0.0023$. The systematic uncertainty due to the choice of the sPlot method as background subtraction method is included in the fitter validation uncertainty. Additional possible sources of systematic uncertainties are considered and found negligible. These include the decay-time dependence of the FT efficiency and of the mistag; the choice of model for the decay-time efficiency, and the validation of the decay-time bias correction method.

Several cross-checks are performed to assess the consistency of the results by splitting the data by K_S^0 reconstruction categories, years of data taking, SS and OS tagging amongst several others. In addition, the fits are performed in bins of B -meson momentum, pseudorapidity, and other variables correlated to FT performance. The results are also stable against variations of the mass-fit model and the choice of figure of merit used to determine the optimal BDT requirement. Furthermore, the result is unaffected by the specific description of the decay-time efficiency. The decay-time resolution and its modeling only play a minor role in this measurement due to the high decay-time resolution of the LHCb detector and the comparatively slow B^0 oscillation. The choice of decay-time resolution model therefore does not affect the result. The influence of the correlation of invariant mass and decay time was found to be negligible. Several alternative approaches to determine CP -violating parameters are also performed and are consistent with the baseline results. These include the determination of S and C parameters from the time-integrated asymmetry, a fit based on different assumptions on the normalizations of the B^0 and \bar{B}^0 amplitudes, and a statistical method to determine CP -violation parameters using a model-independent approach to account for the decay-time efficiency.

The CP -violation parameters are measured to be

$$\begin{aligned}
S_{J/\psi(\rightarrow\mu^+\mu^-)K_S^0} &= 0.716 \pm 0.015 \text{ (stat)} \pm 0.007 \text{ (syst)}, \\
C_{J/\psi(\rightarrow\mu^+\mu^-)K_S^0} &= 0.010 \pm 0.014 \text{ (stat)} \pm 0.003 \text{ (syst)}, \\
S_{\psi(2S)(\rightarrow\mu^+\mu^-)K_S^0} &= 0.649 \pm 0.053 \text{ (stat)} \pm 0.018 \text{ (syst)}, \\
C_{\psi(2S)(\rightarrow\mu^+\mu^-)K_S^0} &= -0.087 \pm 0.048 \text{ (stat)} \pm 0.005 \text{ (syst)}, \\
S_{J/\psi(\rightarrow e^+e^-)K_S^0} &= 0.754 \pm 0.037 \text{ (stat)} \pm 0.008 \text{ (syst)}, \\
C_{J/\psi(\rightarrow e^+e^-)K_S^0} &= 0.042 \pm 0.034 \text{ (stat)} \pm 0.008 \text{ (syst)}.
\end{aligned}$$

The corresponding correlation coefficients between S and C are 0.446, 0.503, and 0.374 for $J/\psi(\rightarrow\mu^+\mu^-)$, $\psi(2S)(\rightarrow\mu^+\mu^-)$, and $J/\psi(\rightarrow e^+e^-)$ final states, respectively. A combined fit of the $B^0 \rightarrow J/\psi(\mu\mu)K_S^0$ and $B^0 \rightarrow J/\psi(\rightarrow ee)K_S^0$ modes results in

$$\begin{aligned}
S_{J/\psi K_S^0} &= 0.722 \pm 0.014 \text{ (stat)} \pm 0.007 \text{ (syst)}, \\
C_{J/\psi K_S^0} &= 0.015 \pm 0.013 \text{ (stat)} \pm 0.003 \text{ (syst)},
\end{aligned}$$

with a correlation coefficient of 0.437. A simultaneous fit of the three decay modes is performed and results in

$$\begin{aligned}
S_{\psi K_S^0} &= 0.717 \pm 0.013 \text{ (stat)} \pm 0.008 \text{ (syst)}, \\
C_{\psi K_S^0} &= 0.008 \pm 0.012 \text{ (stat)} \pm 0.003 \text{ (syst)},
\end{aligned}$$

with a correlation coefficient of 0.441. Finally, a combination of the LHCb Run 1 and Run 2 results is performed. It is assumed that sources of systematic uncertainties from external parameters Δm_d , $\Delta\Gamma_d$, and α are fully correlated between these measurements. The combination of measurements yields

$$\begin{aligned}
S_{\psi K_S^0}^{\text{Run 1\&2}} &= 0.724 \pm 0.014 \text{ (stat+syst)}, \\
C_{\psi K_S^0}^{\text{Run 1\&2}} &= 0.004 \pm 0.012 \text{ (stat+syst)},
\end{aligned}$$

with a correlation coefficient of 0.40, and for final states that contain a J/ψ meson the combination is

$$\begin{aligned}
S_{J/\psi K_S^0}^{\text{Run 1\&2}} &= 0.726 \pm 0.014 \text{ (stat+syst)}, \\
C_{J/\psi K_S^0}^{\text{Run 1\&2}} &= 0.010 \pm 0.012 \text{ (stat+syst)},
\end{aligned}$$

with a correlation coefficient of 0.41.

In summary, a measurement of time-dependent CP violation in $B^0 \rightarrow J/\psi(\rightarrow\mu^+\mu^-)K_S^0$, $B^0 \rightarrow \psi(2S)(\rightarrow\mu^+\mu^-)K_S^0$, and $B^0 \rightarrow J/\psi(\rightarrow e^+e^-)K_S^0$ decays using the full LHCb Run 2 data corresponding to an integrated luminosity of 6 fb^{-1} from pp collisions at a center-of-mass energy of 13 TeV is reported. These measurements are in agreement with recent predictions by the CKMfitter group [35] and the UTfit group [36] and the current world averages as reported by HFLAV [1]. The result of the simultaneous fit to all channels is more precise than the current HFLAV world average.

Acknowledgements

We express our gratitude to our colleagues in the CERN accelerator departments for the excellent performance of the LHC. We thank the technical and administrative staff at the LHCb institutes. We acknowledge support from CERN and from the national agencies: CAPES, CNPq, FAPERJ and FINEP (Brazil); MOST and NSFC (China); CNRS/IN2P3 (France); BMBF, DFG and MPG (Germany); INFN (Italy); NWO (Netherlands); MNiSW and NCN (Poland); MCID/IFA (Romania); MICINN (Spain); SNSF and SER (Switzerland); NASU (Ukraine); STFC (United Kingdom); DOE NP and NSF (USA). We acknowledge the computing resources that are provided by CERN, IN2P3 (France), KIT and DESY (Germany), INFN (Italy), SURF (Netherlands), PIC (Spain), GridPP (United Kingdom), CSCS (Switzerland), IFIN-HH (Romania), CBPF (Brazil), Polish WLCG (Poland) and NERSC (USA). We are indebted to the communities behind the multiple open-source software packages on which we depend. Individual groups or members have received support from ARC and ARDC (Australia); Minciencias (Colombia); AvH Foundation (Germany); EPLANET, Marie Skłodowska-Curie Actions, ERC and NextGenerationEU (European Union); A*MIDEX, ANR, IPhU and Labex P2IO, and Région Auvergne-Rhône-Alpes (France); Key Research Program of Frontier Sciences of CAS, CAS PIFI, CAS CCEPP, Fundamental Research Funds for the Central Universities, and Sci. & Tech. Program of Guangzhou (China); GVA, XuntaGal, GENCAT, Inditex, InTalent and Prog. Atracción Talento, CM (Spain); SRC (Sweden); the Leverhulme Trust, the Royal Society and UKRI (United Kingdom).

References

- [1] Y. Amhis *et al.*, *Averages of b -hadron, c -hadron, and τ -lepton properties as of 2021*, Phys. Rev. **D107** (2023) 052008, [arXiv:2206.07501](https://arxiv.org/abs/2206.07501), updated results and plots available at <https://hflav.web.cern.ch>.
- [2] BABAR collaboration, B. Aubert *et al.*, *Observation of CP violation in the B^0 meson system*, Phys. Rev. Lett. **87** (2001) 091801.
- [3] Belle collaboration, K. Abe *et al.*, *Observation of large CP violation in the neutral B meson system*, Phys. Rev. Lett. **87** (2001) 091802.
- [4] BABAR collaboration, B. Aubert *et al.*, *Measurement of time-dependent CP asymmetry in $B^0 \rightarrow c\bar{c}K^{(*)0}$ decays*, Phys. Rev. **D79** (2009) 072009, [arXiv:0902.1708](https://arxiv.org/abs/0902.1708).
- [5] Belle collaboration, I. Adachi *et al.*, *Precise measurement of the CP violation parameter $\sin 2\phi_1$ in $B^0 \rightarrow (c\bar{c})K^0$ decays*, Phys. Rev. Lett. **108** (2012) 171802, [arXiv:1201.4643](https://arxiv.org/abs/1201.4643).
- [6] LHCb collaboration, R. Aaij *et al.*, *Measurement of CP violation in $B^0 \rightarrow J/\psi K_S^0$ decays*, Phys. Rev. Lett. **115** (2015) 031601, [arXiv:1503.07089](https://arxiv.org/abs/1503.07089).
- [7] LHCb collaboration, R. Aaij *et al.*, *Measurement of CP violation in $B^0 \rightarrow J/\psi K_S^0$ and $B^0 \rightarrow \psi(2S)K_S^0$ decays*, JHEP **11** (2017) 170, [arXiv:1709.03944](https://arxiv.org/abs/1709.03944).

- [8] Belle II collaboration, I. Adachi *et al.*, *Measurement of decay-time-dependent CP violation in $B^0 \rightarrow J/\psi K_S^0$ decays using 2019-2021 Belle II data*, arXiv:2302.12898.
- [9] T. Gershon and Y. Nir, *CP violation in the quark sector*, 2022. review in Ref. [10].
- [10] Particle Data Group, R. L. Workman *et al.*, *Review of particle physics*, Prog. Theor. Exp. Phys. **2022** (2022) 083C01.
- [11] K. De Bruyn and R. Fleischer, *A roadmap to control penguin effects in $B_d^0 \rightarrow J/\psi K_S^0$ and $B_s^0 \rightarrow J/\psi \phi$* , JHEP **03** (2015) 145, arXiv:1412.6834.
- [12] M. Z. Barel, K. De Bruyn, R. Fleischer, and E. Malami, *In pursuit of new physics with $B_d^0 \rightarrow J/\psi K^0$ and $B_s^0 \rightarrow J/\psi \phi$ decays at the high-precision frontier*, J. Phys. **G48** (2021) 065002, arXiv:2010.14423.
- [13] M. Ciuchini, M. Pierini, and L. Silvestrini, *Effect of penguin operators in the $B^0 \rightarrow J/\psi K^0$ CP asymmetry*, Phys. Rev. Lett. **95** (2005) 221804.
- [14] S. Faller, M. Jung, R. Fleischer, and T. Mannel, *The golden modes $B^0 \rightarrow J/\psi K_{S,L}$ in the era of precision flavour physics*, Phys. Rev. **D79** (2009) 014030, arXiv:0809.0842.
- [15] M. Jung, *Determining weak phases from $B \rightarrow J/\psi P$ decays*, Phys. Rev. **D86** (2012) 053008, arXiv:1206.2050.
- [16] P. Frings, U. Nierste, and M. Wiebusch, *Penguin contributions to CP phases in $B_{d,s}$ decays to charmonium*, Phys. Rev. Lett. **115** (2015) 061802, arXiv:1503.00859.
- [17] LHCb collaboration, A. A. Alves Jr. *et al.*, *The LHCb detector at the LHC*, JINST **3** (2008) S08005.
- [18] LHCb collaboration, R. Aaij *et al.*, *LHCb detector performance*, Int. J. Mod. Phys. **A30** (2015) 1530022, arXiv:1412.6352.
- [19] R. Aaij *et al.*, *The LHCb trigger and its performance in 2011*, JINST **8** (2013) P04022, arXiv:1211.3055.
- [20] T. Chen and C. Guestrin, *XGBoost (version 1.0.2): A scalable tree boosting system*, in *Proceedings of the 22nd ACM SIGKDD International Conference on Knowledge Discovery and Data Mining KDD '16* (2016) 785–794, arXiv:1603.02754.
- [21] T. Sjöstrand, S. Mrenna, and P. Skands, *A brief introduction to PYTHIA 8.1*, Comput. Phys. Commun. **178** (2008) 852, arXiv:0710.3820; T. Sjöstrand, S. Mrenna, and P. Skands, *PYTHIA 6.4 physics and manual*, JHEP **05** (2006) 026, arXiv:hep-ph/0603175.
- [22] I. Belyaev *et al.*, *Handling of the generation of primary events in Gauss, the LHCb simulation framework*, J. Phys. Conf. Ser. **331** (2011) 032047.
- [23] Geant4 collaboration, J. Allison *et al.*, *Geant4 developments and applications*, IEEE Trans. Nucl. Sci. **53** (2006) 270; Geant4 collaboration, S. Agostinelli *et al.*, *Geant4: A simulation toolkit*, Nucl. Instrum. Meth. **A506** (2003) 250.

- [24] D. J. Lange, *The EvtGen particle decay simulation package*, Nucl. Instrum. Meth. **A462** (2001) 152.
- [25] N. Davidson, T. Przedzinski, and Z. Was, *PHOTOS interface in C++: Technical and physics documentation*, Comp. Phys. Comm. **199** (2016) 86, [arXiv:1011.0937](https://arxiv.org/abs/1011.0937).
- [26] A. Blum, A. T. Kalai, and J. Langford, *Beating the hold-out: bounds for k-fold and progressive cross-validation*, in *Proceedings of the twelfth annual conference on computational learning theory*, Association for Computing Machinery, New York, 1999.
- [27] LHCb collaboration, R. Aaij *et al.*, *Opposite-side flavour tagging of B mesons at the LHCb experiment*, Eur. Phys. J. **C72** (2012) 2022, [arXiv:1202.4979](https://arxiv.org/abs/1202.4979).
- [28] D. Fazzini, *Flavour Tagging in the LHCb experiment*, in *Proceedings, 6th Large Hadron Collider Physics Conference (LHCP 2018): Bologna, Italy, 2018*, Proceedings of Science (PoS), Bologna, Italy, 2018 **LHCP2018** 230.
- [29] Q. Fühling and V. Jevtić, *lhcb-ftcalib (version 1.4.0): LHCb Flavour Tagging calibration software*, 2022. https://gitlab.cern.ch/lhcb-ft/lhcb_ftcalib.
- [30] M. Pivk and F. R. Le Diberder, *sPlot: A statistical tool to unfold data distributions*, Nucl. Instrum. Meth. **A555** (2005) 356, [arXiv:physics/0402083](https://arxiv.org/abs/physics/0402083).
- [31] Y. Xie, *sFit: a method for background subtraction in maximum likelihood fit*, [arXiv:0905.0724](https://arxiv.org/abs/0905.0724).
- [32] D. Martínez Santos and F. Dupertuis, *Mass distributions marginalized over per-event errors*, Nucl. Instrum. Meth. **A764** (2014) 150, [arXiv:1312.5000](https://arxiv.org/abs/1312.5000).
- [33] W. Fetscher *et al.*, *Regeneration of arbitrary coherent neutral kaon states: A new method for measuring the K^0 - \bar{K}^0 forward scattering amplitude*, Z. Phys. **C72** (1996) 543.
- [34] B. R. Ko, E. Won, B. Golob, and P. Pakhlov, *Effect of nuclear interactions of neutral kaons on CP asymmetry measurements*, Phys. Rev. **D84** (2011) 111501, [arXiv:1006.1938](https://arxiv.org/abs/1006.1938).
- [35] CKMfitter group, J. Charles *et al.*, *Current status of the standard model CKM fit and constraints on $\Delta F = 2$ new physics*, Phys. Rev. **D91** (2015) 073007, [arXiv:1501.05013](https://arxiv.org/abs/1501.05013), updated results and plots available at <http://ckmfitter.in2p3.fr/>.
- [36] UTfit collaboration, M. Bona *et al.*, *The unitarity triangle fit in the standard model and hadronic parameters from lattice QCD: A reappraisal after the measurements of Δm_s and $BR(B \rightarrow \tau\nu_\tau)$* , JHEP **10** (2006) 081, [arXiv:hep-ph/0606167](https://arxiv.org/abs/hep-ph/0606167), updated results and plots available at <http://www.utfit.org/>.

- ³⁴ *Nikhef National Institute for Subatomic Physics and VU University Amsterdam, Amsterdam, Netherlands*
- ³⁵ *AGH - University of Science and Technology, Faculty of Physics and Applied Computer Science, Kraków, Poland*
- ³⁶ *Henryk Niewodniczanski Institute of Nuclear Physics Polish Academy of Sciences, Kraków, Poland*
- ³⁷ *National Center for Nuclear Research (NCBJ), Warsaw, Poland*
- ³⁸ *Horia Hulubei National Institute of Physics and Nuclear Engineering, Bucharest-Magurele, Romania*
- ³⁹ *Affiliated with an institute covered by a cooperation agreement with CERN*
- ⁴⁰ *DS4DS, La Salle, Universitat Ramon Llull, Barcelona, Spain*
- ⁴¹ *ICCUB, Universitat de Barcelona, Barcelona, Spain*
- ⁴² *Instituto Galego de Física de Altas Enerxías (IGFAE), Universidade de Santiago de Compostela, Santiago de Compostela, Spain*
- ⁴³ *Instituto de Física Corpuscular, Centro Mixto Universidad de Valencia - CSIC, Valencia, Spain*
- ⁴⁴ *European Organization for Nuclear Research (CERN), Geneva, Switzerland*
- ⁴⁵ *Institute of Physics, Ecole Polytechnique Fédérale de Lausanne (EPFL), Lausanne, Switzerland*
- ⁴⁶ *Physik-Institut, Universität Zürich, Zürich, Switzerland*
- ⁴⁷ *NSC Kharkiv Institute of Physics and Technology (NSC KIPT), Kharkiv, Ukraine*
- ⁴⁸ *Institute for Nuclear Research of the National Academy of Sciences (KINR), Kyiv, Ukraine*
- ⁴⁹ *University of Birmingham, Birmingham, United Kingdom*
- ⁵⁰ *H.H. Wills Physics Laboratory, University of Bristol, Bristol, United Kingdom*
- ⁵¹ *Cavendish Laboratory, University of Cambridge, Cambridge, United Kingdom*
- ⁵² *Department of Physics, University of Warwick, Coventry, United Kingdom*
- ⁵³ *STFC Rutherford Appleton Laboratory, Didcot, United Kingdom*
- ⁵⁴ *School of Physics and Astronomy, University of Edinburgh, Edinburgh, United Kingdom*
- ⁵⁵ *School of Physics and Astronomy, University of Glasgow, Glasgow, United Kingdom*
- ⁵⁶ *Oliver Lodge Laboratory, University of Liverpool, Liverpool, United Kingdom*
- ⁵⁷ *Imperial College London, London, United Kingdom*
- ⁵⁸ *Department of Physics and Astronomy, University of Manchester, Manchester, United Kingdom*
- ⁵⁹ *Department of Physics, University of Oxford, Oxford, United Kingdom*
- ⁶⁰ *Massachusetts Institute of Technology, Cambridge, MA, United States*
- ⁶¹ *University of Cincinnati, Cincinnati, OH, United States*
- ⁶² *University of Maryland, College Park, MD, United States*
- ⁶³ *Los Alamos National Laboratory (LANL), Los Alamos, NM, United States*
- ⁶⁴ *Syracuse University, Syracuse, NY, United States*
- ⁶⁵ *School of Physics and Astronomy, Monash University, Melbourne, Australia, associated to ⁵²*
- ⁶⁶ *Pontifícia Universidade Católica do Rio de Janeiro (PUC-Rio), Rio de Janeiro, Brazil, associated to ²*
- ⁶⁷ *Physics and Micro Electronic College, Hunan University, Changsha City, China, associated to ⁷*
- ⁶⁸ *Guangdong Provincial Key Laboratory of Nuclear Science, Guangdong-Hong Kong Joint Laboratory of Quantum Matter, Institute of Quantum Matter, South China Normal University, Guangzhou, China, associated to ³*
- ⁶⁹ *Lanzhou University, Lanzhou, China, associated to ⁴*
- ⁷⁰ *School of Physics and Technology, Wuhan University, Wuhan, China, associated to ³*
- ⁷¹ *Departamento de Física, Universidad Nacional de Colombia, Bogota, Colombia, associated to ¹⁴*
- ⁷² *Universität Bonn - Helmholtz-Institut für Strahlen und Kernphysik, Bonn, Germany, associated to ¹⁸*
- ⁷³ *Eotvos Lorand University, Budapest, Hungary, associated to ⁴⁴*
- ⁷⁴ *INFN Sezione di Perugia, Perugia, Italy, associated to ²²*
- ⁷⁵ *Van Swinderen Institute, University of Groningen, Groningen, Netherlands, associated to ³³*
- ⁷⁶ *Universiteit Maastricht, Maastricht, Netherlands, associated to ³³*
- ⁷⁷ *Tadeusz Kosciuszko Cracow University of Technology, Cracow, Poland, associated to ³⁶*
- ⁷⁸ *Department of Physics and Astronomy, Uppsala University, Uppsala, Sweden, associated to ⁵⁵*
- ⁷⁹ *University of Michigan, Ann Arbor, MI, United States, associated to ⁶⁴*
- ⁸⁰ *Departement de Physique Nucleaire (SPhN), Gif-Sur-Yvette, France*

^a *Universidade de Brasília, Brasília, Brazil*

^b *Universidade Federal do Triângulo Mineiro (UFTM), Uberaba-MG, Brazil*

^c *Central South U., Changsha, China*

^d *Hangzhou Institute for Advanced Study, UCAS, Hangzhou, China*

- ^e *LIP6, Sorbonne Universite, Paris, France*
^f *Excellence Cluster ORIGINS, Munich, Germany*
^g *Universidad Nacional Autónoma de Honduras, Tegucigalpa, Honduras*
^h *Università di Bari, Bari, Italy*
ⁱ *Università di Bologna, Bologna, Italy*
^j *Università di Cagliari, Cagliari, Italy*
^k *Università di Ferrara, Ferrara, Italy*
^l *Università di Firenze, Firenze, Italy*
^m *Università di Genova, Genova, Italy*
ⁿ *Università degli Studi di Milano, Milano, Italy*
^o *Università di Milano Bicocca, Milano, Italy*
^p *Università di Padova, Padova, Italy*
^q *Università di Perugia, Perugia, Italy*
^r *Scuola Normale Superiore, Pisa, Italy*
^s *Università di Pisa, Pisa, Italy*
^t *Università della Basilicata, Potenza, Italy*
^u *Università di Roma Tor Vergata, Roma, Italy*
^v *Università di Urbino, Urbino, Italy*
^w *Universidad de Alcalá, Alcalá de Henares , Spain*
^x *Universidade da Coruña, Coruña, Spain*

[†] *Deceased*